Supporting Information

Structural Characterization of Heterogeneous Rh-Au Nanoparticles from a Microwave-Assisted Synthesis

Zhiyao Duan,[†] Janis Timoshenko,[‡] Pranaw Kunal,[†] Stephen House,[¶] Haiqin Wan,[†] Karalee Jarvis,[§] Cecile Bonifacio,[¶] Judith C. Yang,[*,¶,‖] Richard M. Crooks,[*,†,§] Anatoly I. Frenkel,[*,‡] Simon M. Humphrey,[*,†,§] and Graeme Henkelman[*,†,§,⊥]

[†]Department of Chemistry, The University of Texas at Austin, Austin, TX 78712-0165, USA

[‡]Department of Materials Science and Chemical Engineering, Stony Brook University, Stony Brook, NY, 11794-2275 USA

[¶]Department of Chemical and Petroleum Engineering, The University of Pittsburgh, Pittsburgh, PA 15261, USA

[§]Texas Materials Institute, The University of Texas at Austin, Austin, TX 78712-0165, USA

[‖]Department of Physics and Astronomy, The University of Pittsburgh, Pittsburgh, PA 15261, USA

[⊥]Institute for Computational Engineering and Sciences, The University of Texas at Austin, Austin, TX 78712-0165, USA

E-mail: judyyang@pitt.edu; crooks@cm.utexas.edu; anatoly.frenkel@stonybrook.edu; smh@cm.utexas.edu; henkelman@utexas.edu

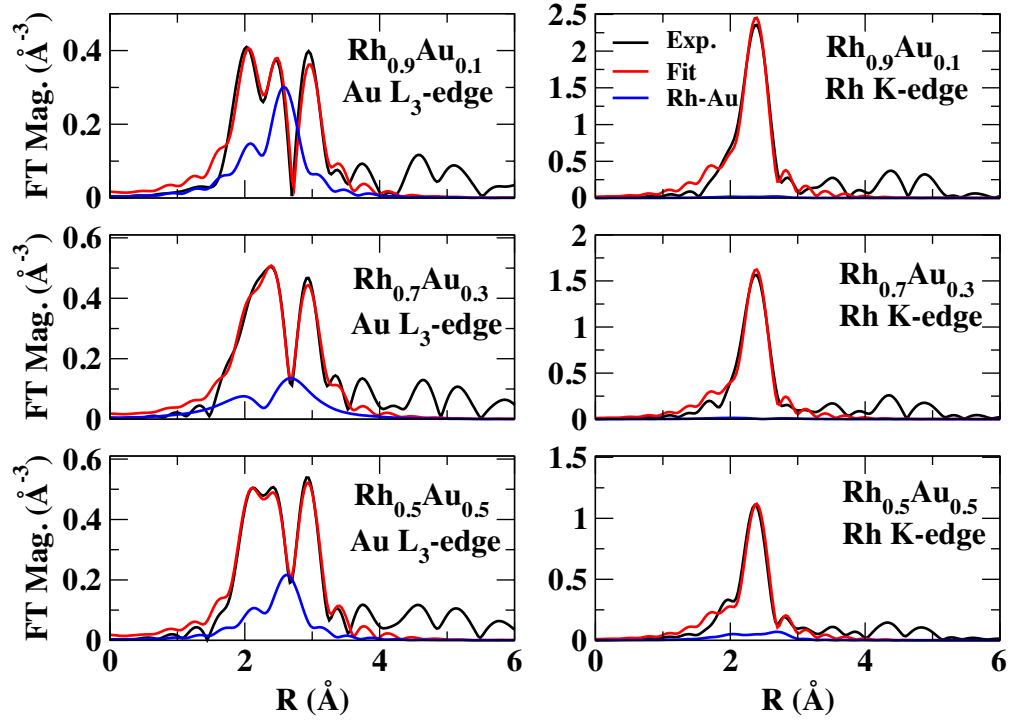# EXAFS fitting to a segregated model

Figure S1: Best-fit for Au L_3-edge and Rh K-edge EXAFS data for $Rh_{0.9}Au_{0.1}$, $Rh_{0.7}Au_{0.3}$, $Rh_{0.5}Au_{0.5}$ NPs. The black curves are the experimental data, the red curves are fits to the experimental data, and the blue curves show the contribution in the fit from Rh-Au scattering.
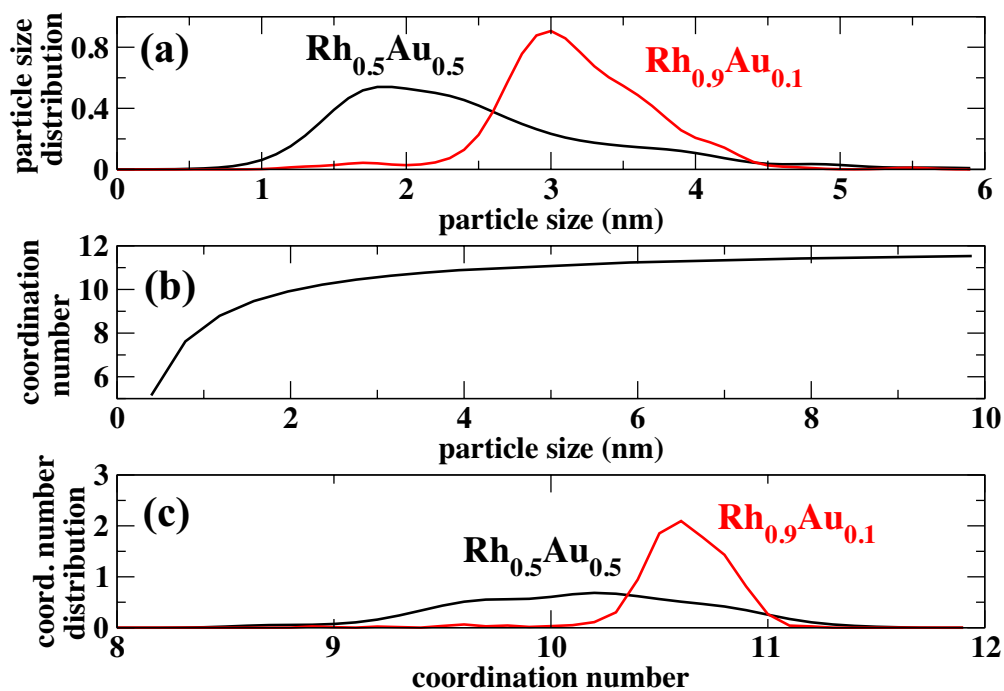
Figure S2: Particle size distributions, obtained from TEM analysis (a) and theoretically expected relation between particle size and average coordination number (b). Panel (c) shows expected distribution of coordination numbers, obtained from results shown in (a) and (b) panels.

4

Empirical potential parameters

Table S1: Parameters of the developed MEAM potentials for Rh-Au alloys. The parameters are the cohesive energy E_c (eV), the equilibrium nearest-neighbor distance (Å), the exponential decay factor for the universal energy function α, the scaling factor for the embedding energy A, the four exponential decay factors for the atomic densities $\beta^{(i)}$, the four weighting factors for the atomic densities $t^{(i)}$ and the density scaling factor ρ^0. The detailed formula of the MEAM potentials could be found in

	E_c	r_e	α	A	$\beta^{(0)}$	$\beta^{(1)}$	$\beta^{(2)}$	$\beta^{(3)}$	$t^{(0)}$	$t^{(1)}$	$t^{(2)}$	$t^{(3)}$	ρ^0
Rh	5.75	2.687	6.00	1.05	4.32	2.00	2.00	5.50	1.00	5.87	4.60	4.80	1.00
Au	3.93	2.885	6.60	1.04	5.55	2.20	2.00	9.00	1.00	3.15	1.51	2.60	1.00
Rh-Au	5.095	2.725	6.20										

Table S2: Angular screening factors of the atomic charge density in the developed MEAM potential for RhAu alloys.

	Rh-Rh-Rh	Rh-Au-Rh	Au-Rh-Rh	Au-Au-Rh	Au-Rh-Au	Au-Au-Au
C_{max}	2.8	2.8	2.8	2.8	2.8	2.8
C_{min}	0.8	0.8	0.8	0.8	0.8	0.8

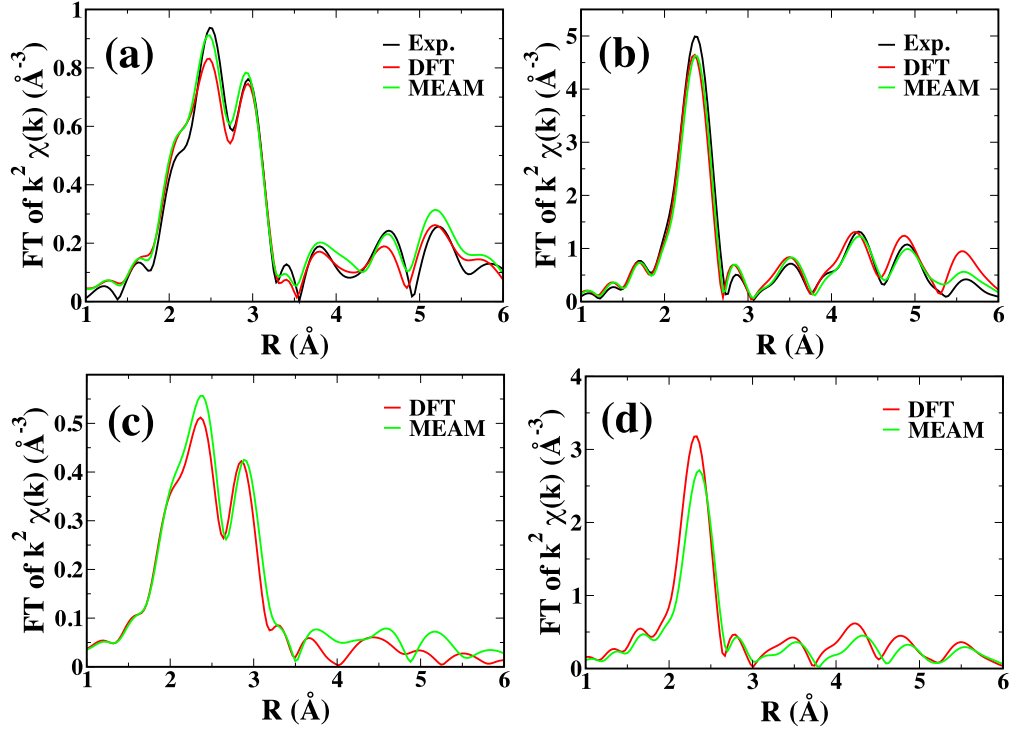# Validation of empirical interatomic potential to EXAFS

Figure S3: Comparison of simulated EXAFS spectra using the developed MEAM potentials with the experimental EXAFS spectra and DFT-derived EXAFS spectra. (a) Au foil (b) Rh foil (c) Au NP201 (d) Rh NP201.

Table S3: Structural parameters obtained by fitting the experimental EXAFS spectra and simulated EXAFS spectra shown in Figure S3.

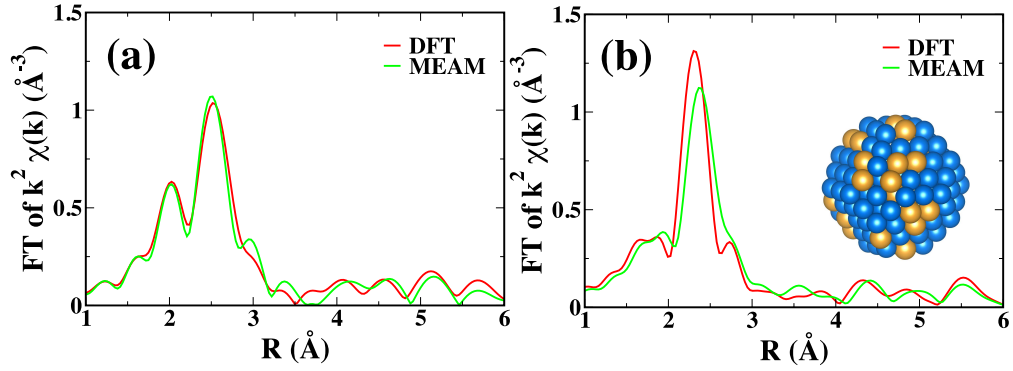|	Au foil			Rh foil			Au NP201		Rh NP201	
	exp.	DFT	MEAM	exp.	DFT	MEAM	DFT	MEAM	DFT	MEAM
N	12	12	12	12	12	12	7.9(1.2)	9.9(1.0)	9.9(4)	9.6(4)
$R(\text{Å})$	2.861(5)	2.889(2)	2.888(2)	2.682(1)	2.671(1)	2.693(1)	2.818(4)	2.842(3)	2.627(1)	2.678(1)
$\sigma^2(10^{-2}\text{Å}^2)$	0.78(2)	0.89(2)	0.84(2)	0.36(2)	0.39(1)	0.38(1)	1.04(11)	1.16(8)	0.51(2)	0.56(2)

Figure S4: Comparison of simulated EXAFS spectra for $Rh_{0.75}Au_{0.25}$ NP201 obtained with the developed MEAM potentials with the EXAFS spectra obtained with DFT. (a) Au L_3-edge (b) Rh K-edge. Blue spheres represent Rh. Gold represent gold.

Table S4: Structural parameters obtained by fitting simulated EXAFS spectra shown in Figure S4.

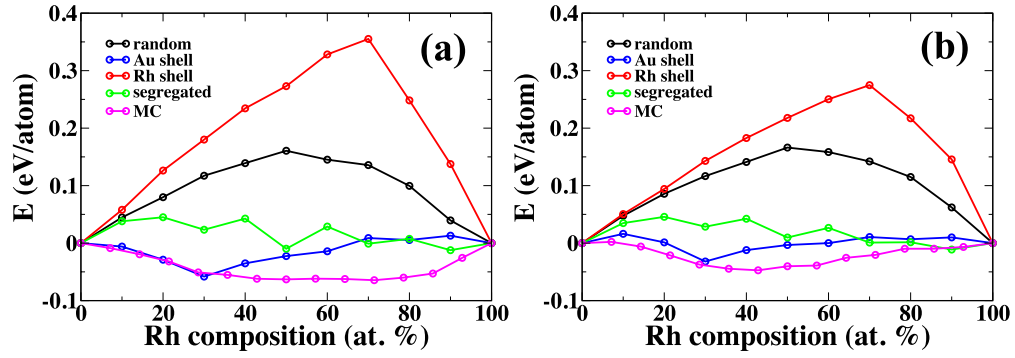|	$Rh_{0.75}Au_{0.25}$ $NP201_{rand}$ Au L_3-edge		$Rh_{0.75}Au_{0.25}$ $NP201_{rand}$ Rh K-edge	
	DFT	MEAM	DFT	MEAM
N_{Au-Au}	2.4(17)	2.4(11)	–	–
N_{Au-Rh}	6.7(9)	6.9(8)	–	–
N_{Rh-Au}	–	–	2.2(8)	2.9(5)
N_{Rh-Rh}	–	–	7.4(8)	7.0(5)
$R_{Au-Au}(\text{Å})$	2.73(3)	2.79(1)	–	–
$R_{Au-Rh}(\text{Å})$	2.705(8)	2.711(6)	–	–
$R_{Rh-Au}(\text{Å})$	–	–	2.705(8)	2.711(6)
$R_{Rh-Rh}(\text{Å})$	–	–	2.633(4)	2.693(3)
$\sigma^2_{Au-Au}(10^{-2}\text{Å}^2)$	0.9(6)	0.7(3)	–	–
$\sigma^2_{Au-Rh}(10^{-2}\text{Å}^2)$	0.8(1)	0.83(8)	–	–
$\sigma^2_{Rh-Au}(10^{-2}\text{Å}^2)$	–	–	0.8(1)	0.83(8)
$\sigma^2_{Rh-Rh}(10^{-2}\text{Å}^2)$	–	–	0.85(6)	0.82(5)

Figure S5: Formation energies of Rh_xAu_{1-x} NP140 of different elemental distributions as a function of Rh composition calculated using (a) DFT (b) MEAM potentials. Examined elemental distributions include random alloy, Au shell (Au atoms are randomly distributed on the surface), Rh shell (Rh atoms are randomly distributed on the surface), segregated (Au and Rh are completely segregated expect for the contact at the interface), and Monte Carlo simulated (MC, the elemental distribution is obatined by MC simulation using the MEAM potentials).
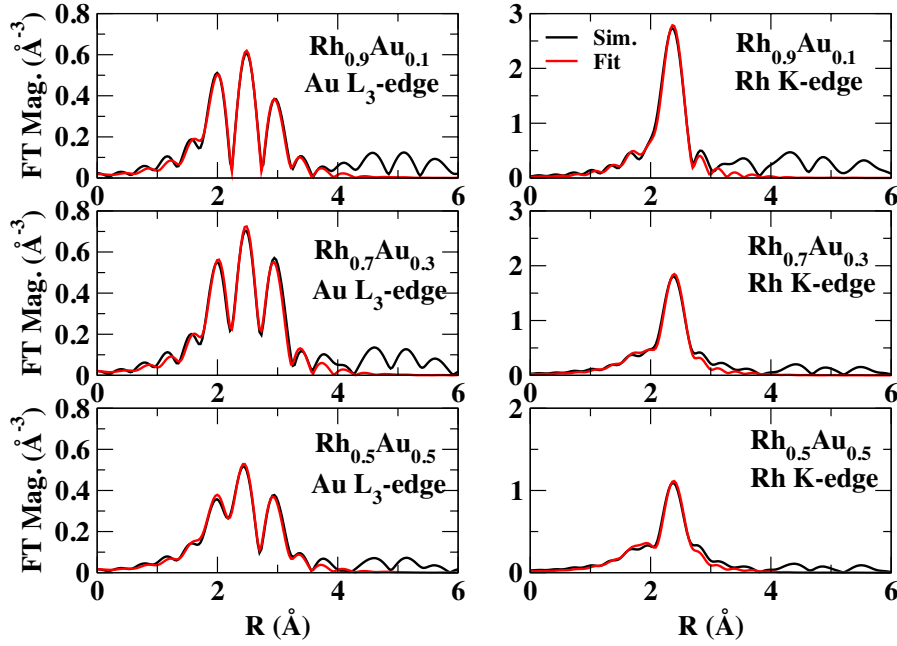
EXAFS comparison to an atomistic model

Figure S6: Best-fit for simulated Au L$_3$-edge and Rh K-edge EXAFS data obtained with single NP models for Rh$_{0.9}$Au$_{0.1}$, Rh$_{0.7}$Au$_{0.3}$, Rh$_{0.5}$Au$_{0.5}$ NPs.

Table S5: Values of structural parameters (Rh–Rh, Rh–Au, Au–Au and Au–Rh coordination numbers N, average distances R and Debye-Waller factors σ^2 for the first coordination shell of Rh and Au atoms in Rh$_{0.9}$Au$_{0.1}$, Rh$_{0.7}$Au$_{0.3}$ and Rh$_{0.5}$Au$_{0.5}$ NPs obtained from the fits of experimental and simulated Au L$_3$-edge and Rh K-edge EXAFS data by single-NP models.

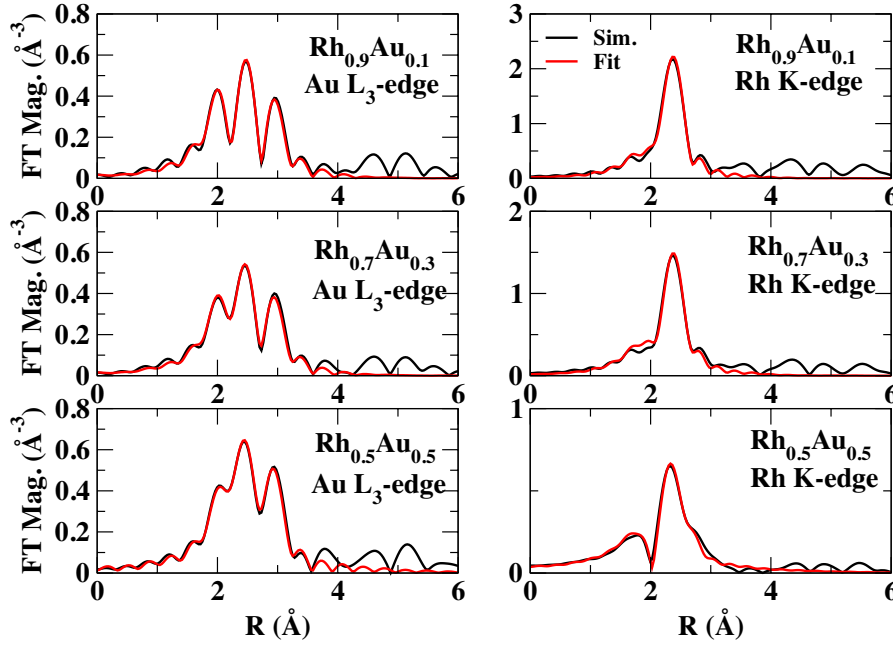|	Rh$_{0.9}$Au$_{0.1}$	Rh$_{0.7}$Au$_{0.3}$	Rh$_{0.5}$Au$_{0.5}$
model	NP586 3NN	NP2406 5NN	NP586 3NN
$N_{\text{Rh－Rh}}$	9.6(8)	9.1(9)	6.2(6)
$N_{\text{Rh－Au}}$	0.4(1)	1.4(5)	2.7(8)
$N_{\text{Au－Au}}$	7(2)	10(2)	9(2)
$N_{\text{Au－Rh}}$	3.8(9)	3(1)	2.7(8)
$R_{\text{Rh－Rh}}(\text{Å})$	2.684(3)	2.703(4)	2.690(4)
$R_{\text{Rh－Au}}(\text{Å})$	2.71(1)	2.72(1)	2.71(1)
$R_{\text{Au－Au}}(\text{Å})$	2.81(1)	2.825(9)	2.819(9)
$R_{\text{Au－Rh}}(\text{Å})$	2.72(1)	2.72(1)	2.71(1)
$\sigma^2_{\text{Rh－Rh}}(10^{-2}\text{Å}^2)$	0.56(4)	0.74(6)	0.80(5)
$\sigma^2_{\text{Rh－Au}}(10^{-2}\text{Å}^2)$	0.7(2)	0.8(3)	1.1(2)
$\sigma^2_{\text{Au－Au}}(10^{-2}\text{Å}^2)$	0.9(2)	0.8(2)	1.0(2)
$\sigma^2_{\text{Au－Rh}}(10^{-2}\text{Å}^2)$	0.7(2)	0.8(3)	1.1(2)

Figure S7: Best-fit for simulated Au L_3-edge and Rh K-edge EXAFS data obtained with bimodal atomistic models for $Rh_{0.9}Au_{0.1}$, $Rh_{0.7}Au_{0.3}$, $Rh_{0.5}Au_{0.5}$ NPs.

Table S6: Values of structural parameters (Rh–Rh, Rh–Au, Au–Au and Au–Rh coordination numbers N, average distances R, and Debye-Waller factors σ^2 for the first coordination shell of Rh and Au atoms in $Rh_{0.9}Au_{0.1}$, $Rh_{0.7}Au_{0.3}$ and $Rh_{0.5}Au_{0.5}$ NPs obtained from the fits of simulated Au L_3-edge and Rh K-edge EXAFS data by bimodal models.

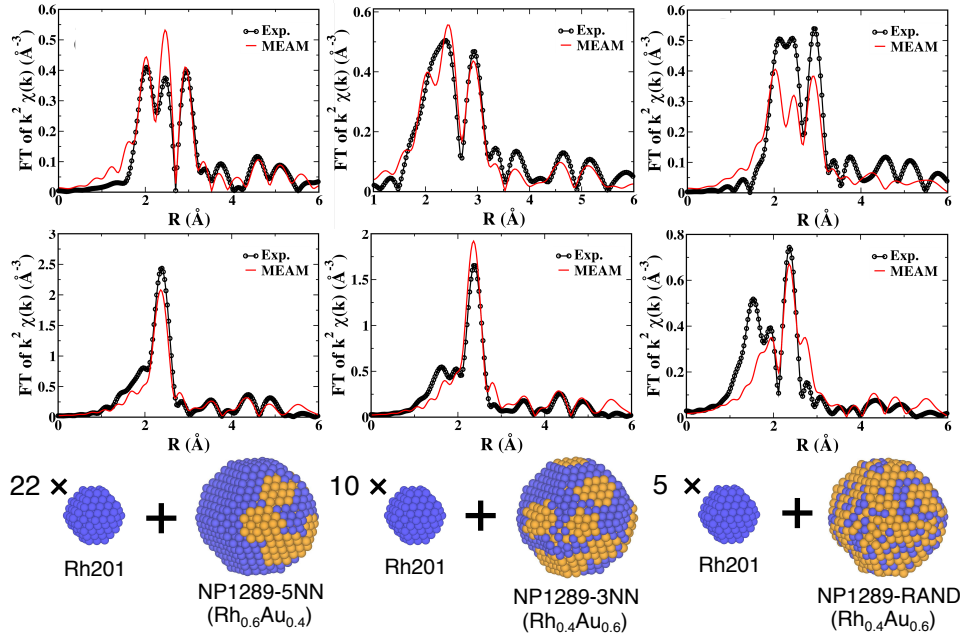|	$Rh_{0.9}Au_{0.1}$	$Rh_{0.7}Au_{0.3}$	$Rh_{0.5}Au_{0.5}$
model	15×Rh38 +	5×Rh38 +	25×Rh38 +
	$Rh_{0.8}Au_{0.2}$ 586 5NN	$Rh_{0.6}Au_{0.4}$ 586 5NN	$Rh_{0.3}Au_{0.7}$ 2406 5NN
N_{Rh-Rh}	8.7(7)	7.2(5)	6.7(8)
N_{Rh-Au}	1(1)	2(1)	2(1)
N_{Au-Au}	8(2)	9(2)	10(2)
N_{Au-Rh}	3(1)	2.2(8)	1.0(6)
$R_{Rh-Rh}(\text{Å})$	2.685(3)	2.684(3)	2.657(7)
$R_{Rh-Au}(\text{Å})$	2.72(1)	2.72(1)	2.71(2)
$R_{Au-Au}(\text{Å})$	2.84(1)	2.833(8)	2.852(9)
$R_{Au-Rh}(\text{Å})$	2.72(1)	2.72(1)	2.71(2)
$\sigma^2_{Rh-Rh}(10^{-2}\text{Å}^2)$	0.62(5)	0.74(5)	1.2(1)
$\sigma^2_{Rh-Au}(10^{-2}\text{Å}^2)$	0.9(2)	0.9(3)	0.8(3)
$\sigma^2_{Au-Au}(10^{-2}\text{Å}^2)$	1.0(2)	1.0(2)	1.0(1)
$\sigma^2_{Au-Rh}(10^{-2}\text{Å}^2)$	0.9(2)	0.9(3)	0.8(3)

Figure S8: Comparison of experimental and simulated Au L$_3$-edge and Rh K-edge EXAFS spectra. The best-fit bimodal models employed to simulate the EXAFS spectra are shown for each case.
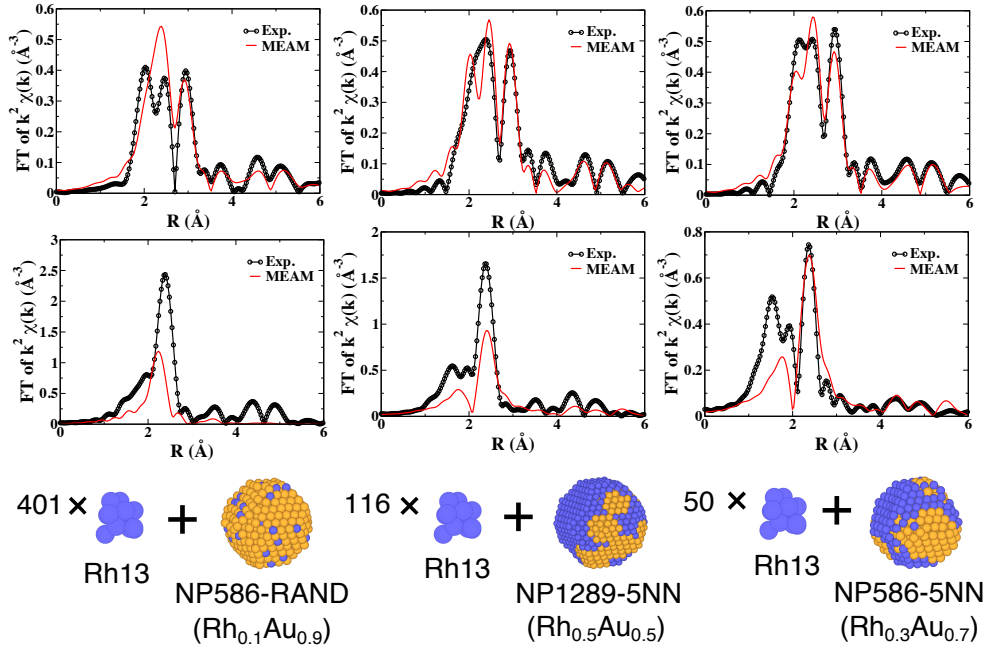

Figure S9: Comparison of experimental and simulated Au L$_3$-edge and Rh K-edge EXAFS spectra. The best-fit bimodal models employed to simulate the EXAFS spectra are shown for each case.